

PREPARED FOR SUBMISSION TO JINST

7TH INTERNATIONAL CONFERENCE ON MICRO-PATTERN GASEOUS DETECTORS
11–16 DECEMBER 2022
REHOVOT, ISRAEL

Performance of the new RD51 VMM3a/SRS beam telescope—studying MPGDs simultaneously in energy, space and time at high rates

L. Scharenberg,^{a,b,1} J. Bortfeldt,^c F. Brunbauer,^a K. Desch,^b K. Flöthner,^{a,d} F. Garcia,^e D. Janssens,^{a,f,g} M. Lisowska,^{a,h} H. Muller,^{b,a} E. Oliveri,^a G. Orlandini,^{a,i} D. Pfeiffer,^{j,k,a} L. Ropelewski,^a J. Samarati,^{j,a} D. Sorvisto,^{l,a} M. van Stenis,^a and R. Veenhof^a

^aEuropean Organization for Nuclear Research (CERN), 1211 Geneva 23, Switzerland

^bPhysikalisches Institut, University of Bonn, Nußallee 12, 53115 Bonn, Germany

^cDepartment for Medical Physics, Ludwig Maximilian University of Munich, Am Coulombwall 1, 85748 Garching, Germany

^dHelmholtz-Institut für Strahlen- und Kernphysik, University of Bonn, Nußallee 14-16, 53115 Bonn, Germany

^eHelsinki Institute of Physics (HIP), P.O. Box 64, FI-00014 University of Helsinki, Finland

^fInter-University Institute For High Energies, Pleinlaan 2, 1050 Brussels, Belgium

^gVrije Universiteit Brussel, Pleinlaan 2, 1050 Brussels, Belgium

^hUniversité Paris-Saclay, 3 rue Joliot Curie, 91190 Gif-sur-Yvette, France

ⁱFriedrich-Alexander-Universität Erlangen-Nürnberg, Schloßplatz 4, 91054 Erlangen, Germany

^jEuropean Spallation Source ERIC (ESS), Box 176, SE-221 00 Lund, Sweden

^kDipartimento di Fisica, University of Milano-Bicocca, Piazza della Scienza 3, 20126 Milan, Italy

^lAalto University, P.O. Box 11000, FI-00076 Aalto, Finland

E-mail: lucian.scharenberg@cern.ch

ABSTRACT: The RD51 collaboration maintains a common infrastructure at CERN for its R & D activities, including two beam telescopes for test beam campaigns. Recently, one of the beam telescopes has been equipped and commissioned with new multi-channel and charge-sensitive front-end electronics based on the ATLAS/BNL VMM3a front-end ASIC and the RD51 Scalable Readout System (SRS). This allows to read out the detectors at high rates (up to the MHz regime) with electronics time resolutions of the order of 1 ns and the ability to handle different detector types and sizes, due to a larger dynamic range compared to the previous front-end electronics based on the APV25 ASIC. Having studied and improved the beam telescope's performance over the course of three test beam campaigns, the results are presented in this paper.

KEYWORDS: Micropattern gaseous detectors (MSGC, GEM, THGEM, RETHGEM, MHSP, MICROPIC, MICROMEGAS, InGrid, etc), Gaseous imaging and tracking detectors, Electronic detector readout concepts (gas, liquid).

¹Corresponding author.

Contents

1	Introduction and system overview	1
2	Performance evaluation	2
2.1	Electronics' rate-capability	2
2.2	Time resolution	2
2.3	Energy/charge information	2
2.4	Particle trajectories: spatial resolution and efficiency	3
3	Improving the spatial resolution	4
4	Conclusion	4

1 Introduction and system overview

As part of its activities, the RD51 collaboration [1] organises up to three test beam campaigns per year at the H4 extraction beam line of the CERN Super Proton Synchrotron (SPS). For this, two beam telescopes are provided, one being based on COMPASS-like triple-GEM detectors [2] and the other on resistive-strip MicroMegas detectors [3].

Both telescopes are equipped with the common RD51 readout electronics—the Scalable Readout System (SRS) [4]—allowing to read out multiple detectors (several thousand readout channels) simultaneously. Following the integration of the ATLAS/BNL VMM3a front-end ASIC [5] into the SRS [6, 7], it replaced the APV25 [8] electronics of the GEM-based telescope. This enables the acquisition of data at much higher rates (MHz regime instead of kHz), with the electronics providing charge and time of the induced signal simultaneously, with the latter being in the nanosecond scale. In addition, different peaking times (25 to 200 ns) and electronics gains (0.5 to 16 mV/fC) can be selected, being useful in the R & D context, as it allows tuning the electronics' settings to the specific detector types. The VMM3a is operated in a self-triggered continuous readout mode, requiring precise clock synchronisation between the front-end cards. This is achieved by using the SRS' Clock and Trigger Fanout (CTF) card.

The telescope contains three triple-GEM detectors ($10 \times 10 \text{ cm}^2$ active area, x - y -strip anode, 256+256 strips at $400 \mu\text{m}$ pitch) over a distance of about 1 m to provide information on the beam particles' trajectories. In addition, it contains three scintillators (two in front of the tracking detectors and one behind them) which are read out with Photo-Multiplier Tubes (PMTs). The output pulses from the PMTs are processed by a NIM-logic including a coincidence unit, which is also read out with VMM3a/SRS. This provides the arrival time of the interacting particles.

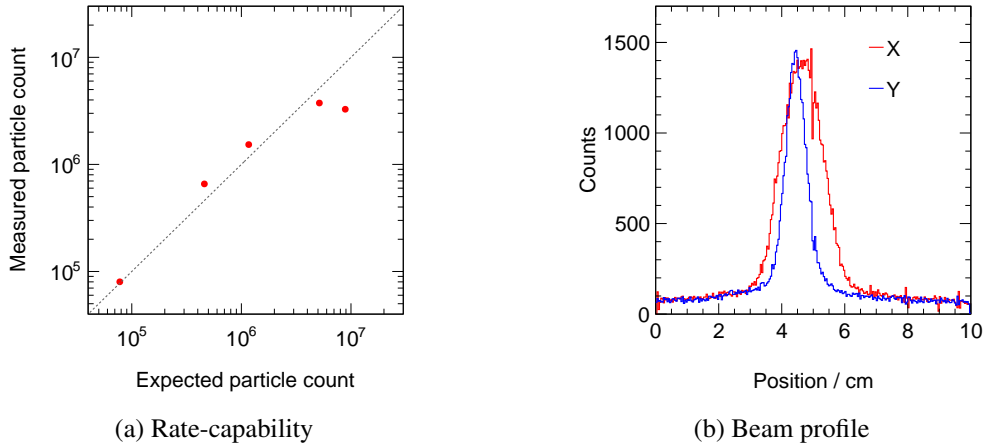


Figure 1: Measured number of particles within a 5 s beam extraction versus the expected one (a). Transverse profile of an 80 GeV/c pion beam with 10^6 particles (b).

2 Performance evaluation

2.1 Electronics' rate-capability

VMM3a/SRS can acquire particle interaction rates in the MHz regime, following studies with X-rays [7]. The same behaviour was observed with Minimum Ionising Particles (MIPs), where the number of particle interactions that can be recorded saturates at around 1 MHz (figure 1a).

This MHz rate-capability—in combination with the triple-GEM detectors—helps for example in understanding the beam structure. While the expected number of particles is provided by the scintillators of the beamline instrumentation even at higher rates, the beam profile measurement of the beamline's delay wire chambers fails at rates $\gtrsim 100$ kHz (figure 1b) due to the rate limits.

2.2 Time resolution

The VMM3a provides the signal arrival time with a resolution between 0.5 and 2 ns [9]. This allows measuring the intrinsic time resolution of MPGDs for tracking without the need of external high-resolution electronics. Using the pulses from the NIM coincidence unit as reference timestamps t_{ref} , it is determined if a particle interaction was recorded by the detector of interest within a previously defined time window (e.g. ± 500 ns) around t_{ref} . The time of the particle interaction is defined as the arrival time of the signal with the largest amplitude t_{LA} [10], as the charge signal is typically spread over several adjacent readout channels. For recorded interactions within the time window, $\Delta t = t_{\text{ref}} - t_{\text{LA}}$ is calculated, resulting in a Gaussian distribution. From the width $\sigma_{\Delta t}$ of this distribution, the detector resolution can be extracted by quadratically subtracting the contributions from the front-end electronics, the NIM-logic and the scintillator/PMTs (figure 2).

2.3 Energy/charge information

The matching in time between the coincidence unit's signals and the tracking detectors allows also for studying the charge/gain/energy behaviour of the detectors. In the given example (figure 2b), the time resolution and charge collection behaviour of a triple-GEM detector are shown.

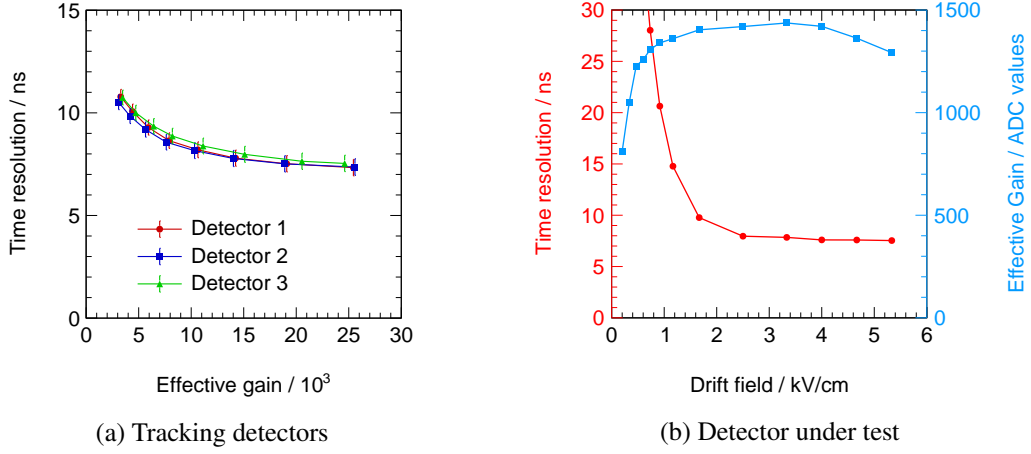


Figure 2: Time resolution of the three tracking detectors, depending on their gain (a). Time resolution of a COMPASS-like triple-GEM detector, depending on the drift field (b).

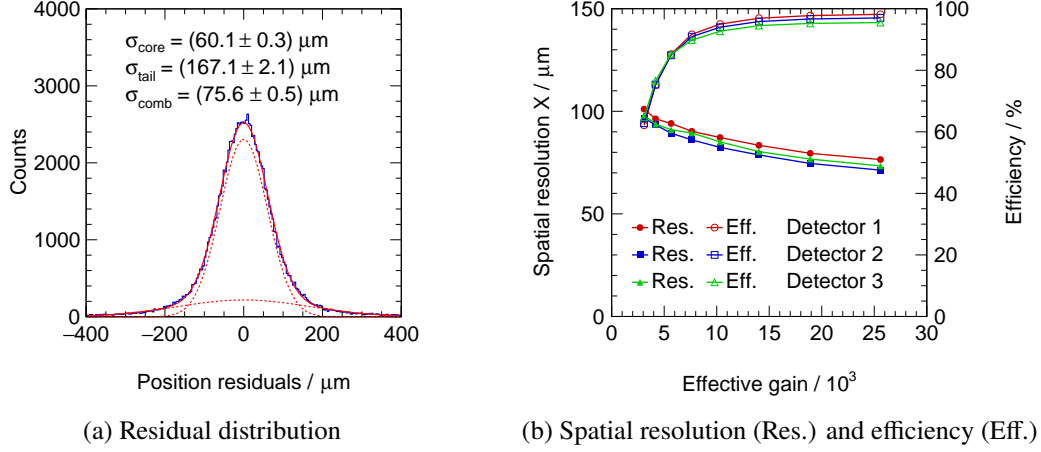


Figure 3: Example of the Δx distribution (a). Spatial resolution and detector efficiency of the three tracking detectors (b).

2.4 Particle trajectories: spatial resolution and efficiency

In the following, the spatial information is added, making use of the three tracking detectors and the reconstruction of the particles' trajectories with a Kalman filter. Due to the self-triggered readout, the events for the track reconstruction are built during the offline analysis, using the recorded interactions in each detector and a time window, similar to the time resolution studies (section 2.2).

To determine the spatial resolution of the tracking detectors, the expected interaction point in the detector of interest x_{ref} is compared with the reconstructed one x' , leading to the distribution of position residuals $\Delta x = x_{\text{ref}} - x'$ (figure 3a). The distribution is fitted with a double-Gaussian function to account for the tails of the residual distribution. The combined width of the residual distribution is determined by $\sigma_{\Delta x}^2 = w\sigma_{\text{centre}}^2 + (1-w)\sigma_{\text{tail}}^2$, with the weighting factor w being the relative scale between the centre and the tail distribution. The detector resolution (figure 3b) is determined by subtracting quadratically the uncertainty of the track reconstruction.

The efficiency of the telescope’s detectors is determined via $\epsilon_{\text{det}} = N_{\text{comb}}/N_{\text{ref}}$, where N_{ref} is the number of expected particles (provided by the reference detectors) and N_{comb} is the number of recorded particle interactions where both, the reference detectors and the detector of interest, participate in the track fit. Only at effective gains $> 10^4$, efficiencies of $> 90\%$ can be reached. The reason for this is the electronics threshold, which in this case was set to 1.5 fC. Due to the system being self-triggered at the threshold level (THL), each signal surpassing the THL is going to be processed, taking part of the available bandwidth. As such, lowering the THL will lead at a certain point to a situation with electronic noise dominating the number of recorded signals. A potential method to overcome the issue with noise acquisition at low threshold levels—still requiring further investigation—is the sub-hysteresis discrimination of the VMM (for details see [11]).

3 Improving the spatial resolution

The telescope provides a precise reference position, making it the ultimate tool for studying improvements in spatial resolution; with a discrete readout structure and threshold-based electronics, charge information is lost, which decreases the accuracy of the position reconstruction when using the centre-of-gravity (COG) method (for details it is referred to [12]). Two approaches—tested previously with X-rays [12]—are the VMM3a’s neighbouring-logic¹ (hardware approach) and changing the Q^2 weighting method² (software approach).

A comparison between the two approaches and the COG results is shown in figure 4a. The neighbouring-logic improves the spatial resolution only in the low signal-to-threshold regime, i.e. at low detector efficiencies. In these situations, the relative amount of charge recovered from below the THL is large, while at higher gains it is significantly lower, also with an increased probability of potentially acquiring noise which would decrease the spatial resolution. The Q^2 weighting on the other hand improves the resolution over the full gain range, also for different threshold levels (figure 4b), allowing to reach resolutions around $50\ \mu\text{m}$.

4 Conclusion

With the integration of the VMM3a front-end ASIC into the RD51 Scalable Readout System, new possibilities opened for detector characterisation studies. The commissioning of a beam telescope with VMM3a/SRS electronics allows studying detectors’ time resolution (better than 10 ns) and position resolution (around $50\ \mu\text{m}$) simultaneously with a single readout system and all data being contained intrinsically in a single data stream. At the same time, due to the increased rate-capability up to the MHz regime, the detector characterisation studies can be performed much faster, allowing to scan a larger range of parameters within a single test beam. It should be noted that while the electronics’ commissioning was performed with COMPASS-like triple-GEM detectors, other detector types (μRWELL [13], resistive-plane MicroMegas, triple-GEM detector with three-layer readout [14] or straw tubes [15]) have been also successfully studied with the new beam telescope and its electronics.

¹When the neighbouring-logic gets enabled and the signal on one channel surpasses the THL, the two adjacent channels are read out as well, even if the signal does not surpass the threshold level.

²In the centre-of-gravity formula, the position is calculated via $x = \sum_i Q_i^n x_i / \sum_i Q_i^n$ with $n = 1$. For the Q^2 weighting, $n = 2$ is used in order to reduce the weight of the tails of the charge distribution (for more details it is referred to [12]).

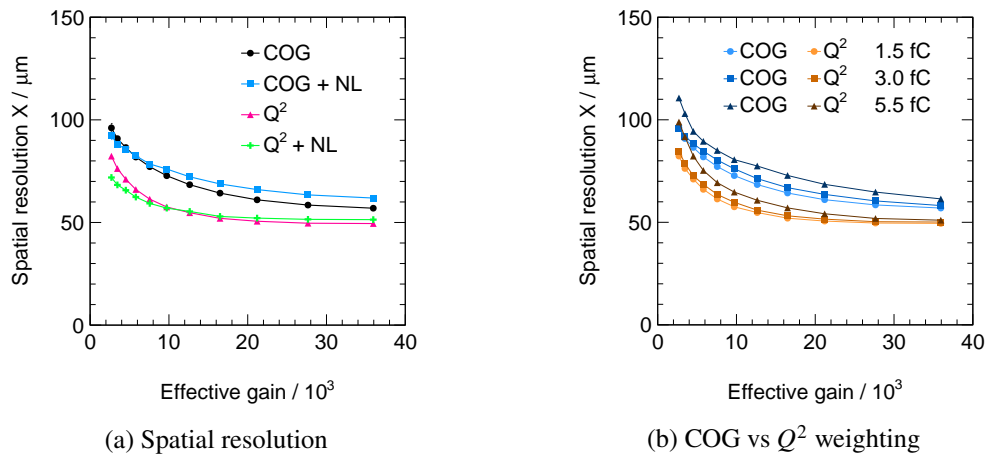


Figure 4: Spatial resolution at an electronics THL of 1.5 fC (a). Comparison between COG and Q^2 reconstruction at different THLs (b).

Acknowledgments

This work has been sponsored by the Wolfgang Gentner Programme of the German Federal Ministry of Education and Research (grant no. 13E18CHA). This project has received funding from the European Union’s Horizon 2020 Research and Innovation programme under Grant Agreement No 101004761. The work has been supported by the CERN Strategic Programme on Technologies for Future Experiments (<https://ep-rnd.web.cern.ch/>). The authors would like to thank Alexandru Rusu (CERN, SRS Technology) for the development and production of the readout electronics.

References

- [1] M. Titov and L. Ropelewski, *Micro-Pattern Gaseous Detector Technologies and RD51 Collaboration*, *Mod. Phys. Lett. A* **28** (2013) 1340022.
DOI: <https://doi.org/10.1142/S0217732313400221>
- [2] C. Altunbas et al., *Construction, test and commissioning of the triple-GEM tracking detector for COMPASS*, *Nucl. Instrum. Meth. A* **490** (2002) 177.
DOI: [https://doi.org/10.1016/S0168-9002\(02\)00910-5](https://doi.org/10.1016/S0168-9002(02)00910-5)
- [3] T. Alexopoulos et al., *A spark-resistant bulk-micromegas chamber for high-rate applications*, *Nucl. Instrum. Meth. A* **640** (2011) 110.
DOI: <https://doi.org/10.1016/j.nima.2011.03.025>
- [4] S. Martoiu, H. Muller, A. Tarazona and J. Toledo, *Development of the scalable readout system for micro-pattern gas detectors and other applications*, *J. Instrum.* **8** (2013) C03015.
DOI: <https://doi.org/10.1088/1748-0221/8/03/C03015>
- [5] G. de Geronimo et al., *The VMM3a ASIC*, *IEEE Trans. Nucl. Sci.* **69** (2022) 976.
DOI: <https://doi.org/10.1109/TNS.2022.3155818>
- [6] M. Lupberger et al., *Implementation of the VMM ASIC in the Scalable Readout System*, *Nucl. Instrum. Meth. A* **903** (2018) 91.

- DOI: <https://doi.org/10.1016/j.nima.2018.06.046>
- [7] D. Pfeiffer, L. Scharenberg, P. Schwäbig et al., *Rate-capability of the VMM3a front-end in the RD51 Scalable Readout System*, *Nucl. Instrum. Meth. A* **1031** (2022) 166548.
DOI: <https://doi.org/10.1016/j.nima.2022.166548>
- [8] M. Raymond et al., *The APV25 0.25 μm CMOS readout chip for the CMS tracker*, *IEEE Nucl. Sci. Symp. Conf. Rec.* **2** (2000) 9/113.
DOI: <https://doi.org/10.1109/NSSMIC.2000.949881>
- [9] L. Scharenberg et al., *Development of a high-rate scalable readout system for gaseous detectors*, *J. Instrum.* **17** (2022) C12014.
DOI: <https://doi.org/10.1088/1748-0221/17/12/C12014>
- [10] D. Pfeiffer et al., *vmm-sdat – VMM3a/SRS Data Analysis Tool*.
URL: <https://github.com/ess-dmhc/vmm-sdat>
- [11] G. de Geronimo et al., *VMM1—An ASIC for Micropattern Detectors*, *IEEE Trans. Nucl. Sci.* **60** (2013) 2314.
DOI: <https://doi.org/10.1109/TNS.2013.2258683>
- [12] L. Scharenberg et al., *X-ray imaging with gaseous detectors using the VMM3a and the SRS*, *Nucl. Instrum. Meth. A* **1011** (2021) 165576.
DOI: <https://doi.org/10.1016/j.nima.2021.165576>
- [13] Y. Zhou et al., *Fabrication and performance of a μRWELL detector with Diamond-Like Carbon resistive electrode and two-dimensional readout*, *Nucl. Instrum. Meth. A* **927** (2019) 31.
DOI: <https://doi.org/10.1016/j.nima.2019.01.036>
- [14] K.J. Flöthner, D. Janssens et al., *The XYU-GEM: Ambiguity-free coordinate readout of the Gas Electron Multiplier*, *Submitted to Nucl. Instrum. Meth. A, RD51-NOTE-2022-09*.
- [15] V. Bautin et al, *VMM3 ASIC as a potential front end electronics solution for future Straw Trackers*, *Nucl. Instrum. Meth. A* **1047** (2023) 167864.
DOI: <https://doi.org/10.1016/j.nima.2022.167864>